Department of Continuum Mechanics | RWTH AACHEN UNIVERSITY

THE PRESENT WORK WAS SUBMITTED TO THE DEPARTMENT OF CONTINUUM MECHANICS

RHEINISCH-WESTFÄLISCHE TECHNISCHE HOCHSCHULE AACHEN
FACULTY OF MECHANICAL ENGINEERING

MASTER THESIS

NONLINEAR MATERIAL PARAMETER IDENTIFICATION OF SOFT MATERIALS BASED ON AN INVERSE FINITE ELEMENT METHOD APPROACH

Presented by:	Nadia Pinedo Oruna, B.Sc.
Study programme:	General Mechanical Engineering M.Sc.
Matriculation number:	397 011
Reviewer:	Univ.-Prof. Dr.-Ing. Mikhail Itskov
Supervisor:	Rasul Abdulsalamov, M.Sc.
External supervisor:	Prof. Kazumi Matsui

Declaration of Authorship

I declare that this work has been composed by myself, and describes my own work, unless otherwise acknowledged in the text.

All sentences or passages quoted in this paper from other people's work have been specifically acknowledged by clear cross-referencing to author, work and page(s). Any photos and illustrations which are not the work of the author have been used with the explicit permission of the originator and are specifically acknowledged.

This work has not been and will not be submitted for any other degree or the obtaining of ECTS points at the RWTH Aachen University or any other institution of higher education.

Aachen, 25th of May 2023

Nadia Pinedo Oruna, B.Sc.

Contents

List of Figures

List of Tables

List of Abbreviations

FEA	**F**inite **E**lement **A**nalysis
FEM	**F**inite **E**lement **M**ethod
iFEM	**i**nverse **F**inite **E**lement **M**ethod
ASME	(The) **A**merican **S**ociety (of) **M**echanical **E**ngineering
TSSA	**T**ransparent **S**tructural **S**ilicone **A**dhesive
PDMS	**P**oly**D**i**M**ethyl**S**iloxane
MAS	**M**inimal **A**ccess **S**urgery
FE	**F**inite **E**lement
NH	**N**eo-**H**ookean
MR	**M**ooney-**R**ivlin
YM	**Y**eoh **M**odel
OM	**O**gden **M**odel

Physical Constants

Speed of Light $c_0 = 2.997\,924\,58 \times 10^8\,\mathrm{m\,s^{-1}}$ (exact)

List of Symbols

A_b	cross-sectional area of the bar	m
A_s	cross-sectional area of the specimen	m
l_s	specimen gauge length	m
C_b	wave speed through the bar	$\mathrm{m\,s^{-1}}$
v_{UC}	testing speed for compression test	$\mathrm{m\,s^{-1}}$
E	Young's Modulus	MPa ($\mathrm{N\,mm^{-2}}$)
S_{ijkl}	compliance tensor	
C_{ijkl}	stiffness tensor	
I_1^*	distortional first invariant	
I_2^*	distortional second invariant	
J	Jacobian of the deformation gradient	
$\boldsymbol{b}^*$	left Cauchy-Green strain tensor	
$\boldsymbol{I}$	identity matrix	
C_{10},C_{01}	Mooney-Rivlin material parameter constants	
C_{10},C_{20},C_{30}	Yeoh model material parameter constants	
$\sigma(t)$	stress	MPa ($\mathrm{N\,mm^{-2}}$)
$\epsilon(t)$	strain	
ϵ_t	transmitted strain signal	
ϵ_r	reflected strain signal	
ϵ_{ij}	strain tensor	
σ_{ij}	stress tensor	
ν	Poisson's ratio	
δ_{ij}	Kronecker delta function	
μ	shear modulus	MPa ($\mathrm{N\,mm^{-2}}$)
λ	Lame's constant	
κ	bulk modulus	MPa ($\mathrm{N\,mm^{-2}}$)
ψ	Helmholtz free energy per unit reference volume	
σ	Cauchy stress	
λ	stretches of the deformation	

1 Introduction

1.1 Background and Problem Statement

The biomechanical characterization of soft tissues has gained attention in medical research [6], in areas such as medical image analysis and visualization. For many years, the obtained medical diagnoses were often based on the assumptions of experts or their accumulated experience. While this information have proven to be useful in general, these methods have limitations in cases where quantifiable data is necessary, specifically for computer-assisted systems, e.g, medical diagnosis, therapy, and training [14]. To gather the material data, e.g., elasticity, stiffness, response under deformation and temperature, it is required to gain access to the soft tissues and perform in vivo testing experiments. However, obtaining accurate biomechanical data can be challenging due to the invasive nature of the procedures and the difficulty in maintaining constant and reproducible internal or external factors in experimental configurations [4].

Especially, when it comes to internal organs, obtaining reliable data for examination after their extraction is difficult because the material properties can vary between samples or testing locations on the same organ [5]. This is due to the influence of various factors such as changes in blood pressure, changes in material properties over time, symptoms of disease, and more. In addition, another problem is the lack of replication, due to the use of different individuals' organs, which introduces more external factors into the equation. Moreover, given a tissue sample, it is difficult to properly characterize the material due to its anisotropic property, which can lead potentially to inaccuracies in the result [6].

In the situation where the material data can be collected in a constant, fast and reliable process, a material model can be established and the computer-aided systems can predict the mechanical behavior of soft tissues, providing preoperative calculations. This demonstrates the importance of material data collection and material model development, especially in the context of computational models such as engineering simulation models created finite element analysis (FEA) software and their medical applications in medical devices, surgical procedures, and training softwares [4]. By using accurate material models, the accuracy of the simulation can be improved, aiding in a better understanding and predicting a soft tissue response to external stimuli [26], making them more useful in medical research and other related applications.

1.2 Objective and Scope of the Study

Soft materials, characterized by low elastic moduli and high sensitivity to external stimuli, frequently experience large deformation and display nonlinear responses [26], making the finite element method (FEM) a common approach for analyzing these materials and solving continuum mechanical problems. Although FEM facilitates the analysis of complex structures with complex material behavior, simulating such materials requires high computational costs.

The main objective of this study is to identify the key parameters of soft materials and their influence on the development of a material model based on inverse finite element method (iFEM) approach. By identifying these key parameters, an attempt is made to approximate the behavior of complex materials through a simplified material model and assess its potential future applications in medical research and its use with organs.

To achieve this goal, an experimental configuration will be selected, and a computational model will be developed to use an iFEM approach to identify the key material parameters of the given soft material. With this method, it was possible to match the results of the computational model to the experimental data, and validate the model with additional data points.

The objective of this study is to develop a framework that identifies the essential material parameters of soft materials and evaluates their limitations and impact on a validated model, which can describe nonlinear material behavior. By contributing to this framework, the study aims to accelerate the development of material models for practical applications in medical research and development.

1.3 State of the Art

This section reviews the state of the art relevant to this study. First, the experimental characterization techniques are reviewed, including methods for obtaining mechanical and viscoelastic properties. This is followed by the description of different approaches to describe the material model for different soft materials. Then, the iFEM, which is one method to identify material parameters from experimental data, will be explained. Finally, the standard verification and validation process used in computational solid mechanics for medical devices based on the American Society of Mechanical Engineering (ASME) guidelines will be discussed. The goal of this chapter is to provide a comprehensive overview of the current methods use in the field and the identification of limitations and gaps in the current state of knowledge.

1.3.1 Experimental Characterization for Soft Materials

Experimental testing is a key approach to obtaining information about the mechanical behavior of soft materials. In order to characterize the mechanical behavior of a test specimen, the most common method method is to mechanically load the specimen and measure the response of the force against the displacement [3]. Soft materials are commonly applied for tissue engineering applications, however, some challenges arise for the design of experimental design due to their elastic modulus range (kPa) and complex mechanical properties [16].

Uniaxial Tension Testing

Uniaxial tension testing are widely employed to determine an stress-strain relationship. For uniaxial tension cases, a specimen is typically loaded by gripping the ends while applying tension, and the deformation is usually measured with a strain gauge

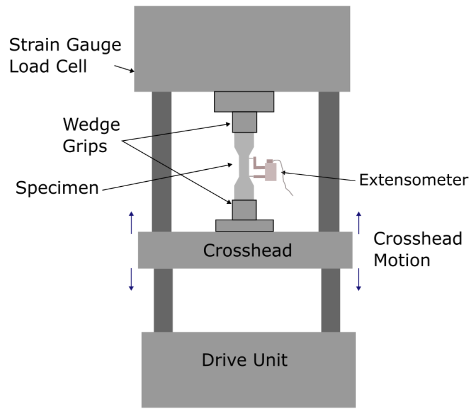

(A) Low strain rate test with a standard tensile machine

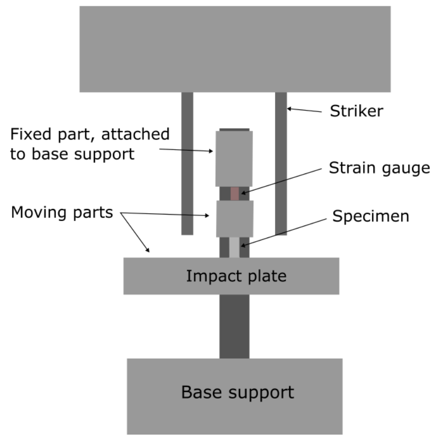

(B) Intermediate strain rate test with a falling weight impact tester

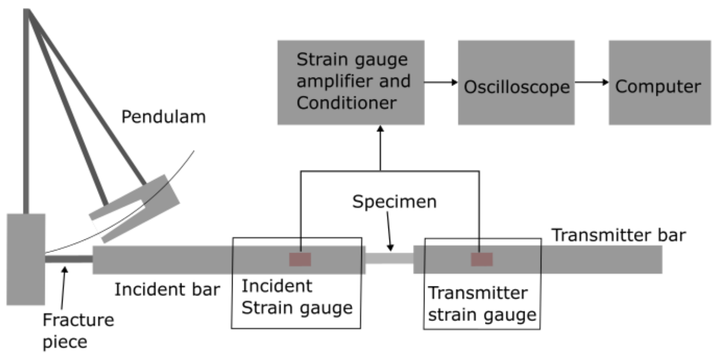

(C) High strain rate test with a split Hopkinson pressure bar in tension

FIGURE 1.1: Uniaxial testing: Diagram of three tensile testing of an ether-based polyurethane elastomer specimen done with three different experiment configurations for different strain rate analysis. Diagrams are based on the study of made by Kayanta and Ivankovic (2010) [13].

[3]. This kind of testing focuses on the central region of the specimen to evade complication arising from ”edge effects”. An homogeneous deformation in the central region is usually expected for this kind of testing, which simplifies the boundary problem and ensures that the measurements represents valid stress-strain values. However, there are two key limitations for uniaxial testing when testing soft materials; first, it may not be suitable when complex boundary conditions arise and is not possible to contro the experimental condition entirely [20]. Second, these tests are inadequate to fully characterize the anisotropic behavior of these materials [6].

In a study made by Kayanta and Ivankovic (2010), the authors investigated the behavior of an ether-based polyurethane elastomer for the creation of mock arteries [13]. Polyurethane was ideal for this application due to its high elasticity and resilience and adaptability to various shapes and sizes. Uniaxial tensile tests on dumbbell-shaped specimens were conducted, divided into three groups based on the strain rate.

For the low strain rate tensile tests (<1/s), a standard Instron machine was utilized, as illustrated in Figure 1.1a. Intermediate strain rate tensile tests (between 1/s and 100/s) were performed using a drop-weight tester (Fig. 1.1b). Load measurements were recorded with a calibrated strain gauge, with the zero position established at the striker and impact plate's initial contact point. High strain rate tests (>100/s) were conducted with a split Hopkinson pressure bar in tension, as shown in Figure 1.1c. A swinging pendulum generated a tensile pulse, propagating along the bar into the specimen. Utilizing the transmitted and reflected strain signals and using the classical Kolsky analysis the specimen stress

$$\sigma(t) = E\frac{A_b}{A_s}\epsilon_t(t)\,,$$

and the strain

$$\epsilon(t) = \frac{-2C_b}{l_s}\int_0^t \epsilon_r(t)dt\,,$$

were calculated. Here, A_b is bar's cross-sectional area, A_s the specimen's cross-sectional area, ϵ_t refers to the transmitted strain signal, ϵ_r is the reflected strain signal, l_s is the specimen gauge length, and C_b is the wave speed through the bar. Low strain rate tests were conducted under dry-room temperature, wet-room temperature, and wet at 37 °C. Intermediate and high strain rate tests were performed exclusively under dry-room temperature conditions.

Test results demonstrated that ether-based polyurethane elastomer specimens were highly sensitive to temperature and humidity, as the material softened with increased levels of these factors. Young's modulus values for dry-room temperature setup 7.4 MPa, decreasing to 5.3 MPa and 4.7 MPa for the wet-room temperature and wet conditions, respectively. Moreover, the polyurethane exhibit varying Young's modulus values under dry-room temperature, depending on the elastomer's composition, with values ranging from 3.6 MPa to 14.8 MPa.

The material displayed minimal strain rate dependency at low strain rates, but exhibited moderate strain rate sensitivity at intermediate and high strain rates, where the Young's modulus ranged between 8 MPa and 12 MPa. However, for strains below 20 %, the outcomes showed repeatability across all strain rates tests.

For strain rates found in arteries around <2/s, the variation of the Young's modulus was insignificant and this could be assumed to be constant. This study demonstrated that it is important to measure the properties of the elastomer under similar condition to the intended application, as properties varies under different conditions.

Uniaxial Compression Testing

Compression tests are also widely utilized to determine the stress-strain response and usually involve placing the specimen in between two plates and compressing the material (Fig. 1.2). The stress-strain response derived from this kind of testing serves in determining the deformation characteristics of the material including the fatigue and fracture resistance. Uniaxial compression tests may be affected by the interface friction between the specimen and the loading plates, leading to a nonhomogeneous deformation state, e.g., barrelling [3].

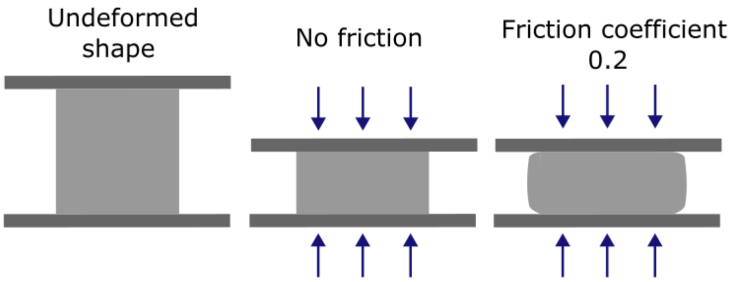

FIGURE 1.2: Uniaxial compression testing: Diagram of typical compression setup and influence of interface friction on the deformed specimen shape [3].

Drass M. et al. conducted a uniaxial compression test, showing that the lubrication was crucial for an homogenous stress and strain distribution. The specimen tested was made from Transparent Structural Silicone Adhesive (TSSA), a rubber-like material commonly used in laminated connections within glass structures. In this study homogeneous and inhomogeneous experiments were performed, as the goal was to determine an experimental setup, which ensured an homogeneous stress and strain distributions for the identification of material parameters [7].

The specimen was compressed with perfect slippage, where the plates and the specimen were lubricated before testing to ensure a frictionless support. A constant speed of $v_{UC} = 0.174\,\mathrm{mm/min}$ was used for this test with a saBesto HHS 5000 machine. The compression test were consucted until a strain $\epsilon = 0.6$ was reached, as the standard deviation for large compression strain ($\epsilon > 0.5$) was too large. The test presented challenges in maintaining the lubrication throughout the test, as it tended to be pressed out between the test specimen and the pressure plates, resulting in a increased friction.

The results of this experiment were processed to identify hyperelastic material parameters using standard fitting routines and inverse methods. The test suggested that only stress-strain response up to a strain value of $\epsilon = 0.5$ should be considered for the indentification of the TSSA material parameters, as the friction's impact can be neglected for smaller strains.

In comparison, for a biomaterials,e.g., human soft tissues, a compressive testing of cartilage was conducted by Griffin M. et al. This study aimed to provide a protocol were compressive and tensile properties of human soft tissues can be evaluated and characterized with minimal destruction. By understanding these material's properties and calculating the Young's elastic modulus, it would be possible to obtain a benchmark for creating suitable tissue-engineered substitutes [10].

The mechanical response of cartilage is highly dependant to the fluid's flow through the tissue. The methods for compression testing can vary with confined or unconfined specimen, and the most prevalent, indentantion (Fig. 1.3). In the unconfined compression the cartilage is pressured using a non-porous plate onto a non-porous chamber, leading to a predominatly radial fluid flow. For the confined compression the sample was placed in a sealed, fluid-filled impermeable chamber and loaded with a porous plate, making the fluid flow restricted to a vertical direction. Finally, the indentation testing employed a smaller indenter applied to the sample's surface perpendicularly, ensuring uniaxial compression and minimizing shear loading. All test were conducted in a hydrated environment and the cartilage

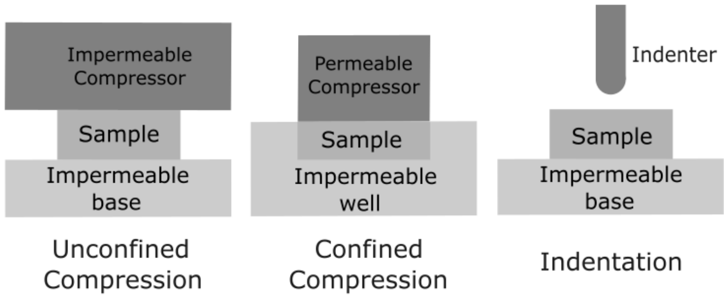

FIGURE 1.3: Uniaxial compression testing: Illustration of different compression methodologies for a cartilage specimen. Unconfined compression, confined compression and Indentation. [10].

was submerged in phosphate-buffered saline before and during the test to maintain the hydration. With the latest compression testing type it was possible to identify elastic and viscoleastic properties of the sample [10].

Indentation

Indentation testing, icluding micro and nanoindentation, is a popular method for characterizing the mechanical properties of soft materials [24]. One of the main advantages of indentation testing is that it requires minimal sample preparation and it is often a nondestructive technique, which allows the preservation of the geometry and tissue's architecture [21]. Furthermore, indentation is useful where more traditional testing techniques such as uniaxial or biaxial testing, are not possible to employ, and can also be utilized to evaluate nonlinear properties, e.g., viscoplastic responses[3].

Despite these advantages, there are some challenges when using indentation to characterize soft materials. First, a stress-strain response is difficult to obtain due to the complex boundary conditions, which introduces an inverse problem for the identification of material parameters [21]. Second, many of the current indentation configurations assume material isotropy, which may not be the case for biomaterials [8]. In addition, determining the mechanical properties of soft materials locally or at small scales is still difficult to achieve [26].

The usual indentation testing setup is shown in Figure 1.4, in this case a system applies a certain force to an attached indenter rod where and specific indenter tip. After the indenter tip goes to a determined displacement, it is possible to obtain a load-displacement curve. The deformation can be measured through an capacitance gauge or also optically, via laser measurements [3].

In a study made by Zhang et al. an investigation of spherical indentation on hyperelastic soft materials was conducted. The material utilized in the experiments was polydimethylsiloxane (PDMS), with was prepared and cured in a cylindrical mold and cured at 60 °C for 8 hours. The ElectroForce 3100 was used to measuring the mechanical properties of PDMS for tensile and indentation tests. Tensile tests were performed to identify the initial shear modulus and locking stretch and their results compared with the indentation tests [26]. For the indentation tests an spherical indenter with a 3 mm radius with a similar configuration shown in Figure 1.4

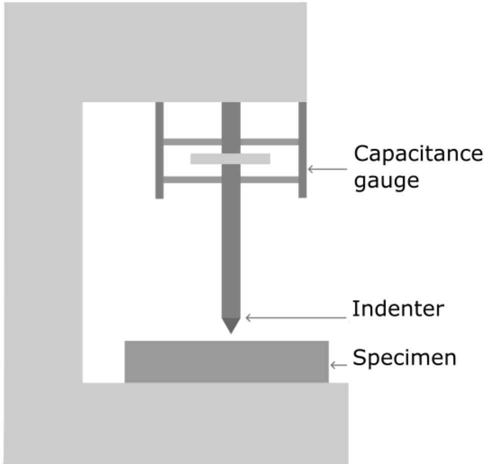

FIGURE 1.4: Nanoindentation experiment setup diagram with an indenter tip attached to a rod and a polymer as specimen [3].

was used. The measurements were done under room temperature and a humidity of 50 % with a loading rate of 2 mm/s and a indentation depth of 3 mm. Six measurements were carried out at different locations on the specimen, generating an indentation load-displacement curves. Moreover, the initial shear modulus was determined using fitted results of the load-depth curves to the Hertzian and hyperelastic solution developed in the study.

The results exhibited that the determination of the initial shear modulus was possible but a certain depth depence coudl be observed. However, a locking stretch could not be analyze due to the sensitivity of these parameters to experimental data noise [26].

For an application with biological tissues Carter et al. performed indentation experiments on human and porcine organs for its application in realistic computer-based simulators for minimal access surgery (MAS) training [4]. This study investigated the stress-strain data pig spleen and liver for ex vivo experiments, along with human liver for in vivo experiments from volunteers patients undergoing a minor surgery. For the ex vivo experiment a static indentation setup was used as shown in Figure 1.5a, where the specimens were placed on a flat surface. A force was applied manually with a winding mechanism at constant rate of 1 mm/s with a rounded indenter with a diameter of 4.5 mm. Ten measurements were carried out on each tissue sample and the load-displacement measurements were gathered with a computerized system with a sampling rate of 15 Hz.

The in vivo experiments were carried out using a hand-held compliance probe. To achieve an overall consistency of the measurements the same surgeon performed the experiments. In addition to maintain consistent indentation depth of 5 mm the indenter was surrounded with a reference ring to provide stability in the measurements (Fig. 1.5b). The force exerted by the weight of the ring was around 0.5 N, while the friction force between the ring and the surface tissue was below 0.05 N, making it a negligible effect. The probe was positioned on the tissue and when the desired indentation depth was indicated with an audible signal. The indentation rate for this configuration ranged from 3 mm/s to 4 mm/s and six measurements

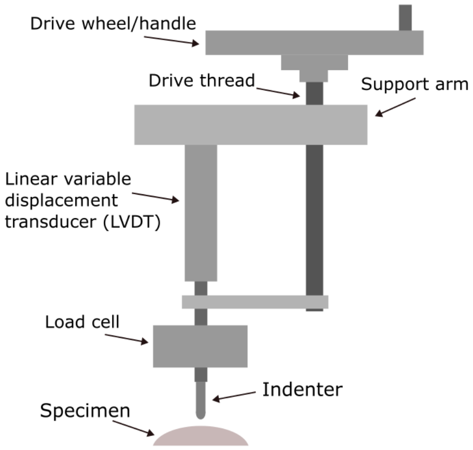

(A) Static indentation configuration used for ex vivo indentations tests. Indenter advances against the tissue by rotating the wheel

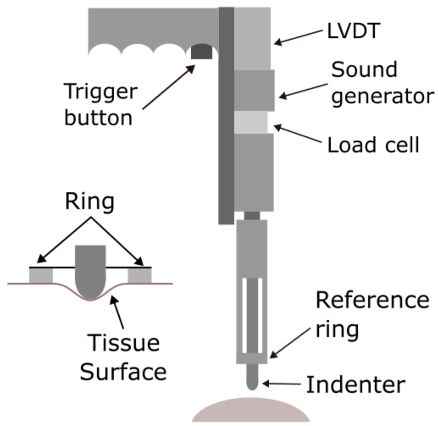

(B) Mobile indentation configuration with outer ring case attached for stabilization of the indentation test.

FIGURE 1.5: Indentation testing: Diagram of static and mobile indentation tests, indenters were attached to a load cell, which was connected to a displacement transducer. Diagrams are based on the study of made by Carter (2001) [4].

were carried out on each patient.

The results were analyzed using MATLAB and showed highly nonlinear stress-strain behavior and large variances. For the reduction of these variances due to the inhomogeneity of the materials and changes over time, the average of the repeated measured was calculated. The measured elastic moduli of pig spleen and liver was 0.11 MPa and 4 MPa respectively, and for the human liver about 0.27 MPa was measured. However, a diseased liver showed a higher elastic modulus of 0.74 MPa [4].

Aspiration Experiment

Tissue aspiration experiments was a method introduced by Kauer (2002) for determining the material parameters of biological soft tissues in vivo. In this study the method was validated with a synthetic material, Silgel, a very soft gel-like material with similar properties to biological soft tissues. This material was ideal to use it for the validation of the aspiration method before applying it to human tissues [14].

The biological sof tissue used in this paper was human uterus. This tissue was selected because it possesses a complex, multilayered structure with anisotropic properties. Moreover, hysterectomy (removal of the uterus) is common surgical procedure, which provides a good chance to perform measurements before and after the removal of the organ.

This method introduced an aspiration tube which is put against the soft tissue, generating a vacuum a causing the deformation of the tissue (Fig.). An advantageous feature of this experimental technique is that it can be perfomed in vivo and ex vivo. With the help of a mirror placed next to aspiration hole, the reflection of the side-view of the tissue can be captured with a video camera. This camera captures the images of the iluminated surface of the material and the aspiration pressure is captured through a sensor. Through this process the captured profile of the tissue is obtained and this can be used to characterize the deformation and analyze the viscoelastic properties of the soft tissue [14].

The main benefits in comparison to more traditional experimental techniques are, the well-defined mechanical boundary conditions during the experiment are executed, large deformation experiments can be assessed, and the viscoelastic properties of the tissue can be analyzed for real surgical procedures due to the time dependent resolution of the deformation.

The results from these experiments corroborates that the development of experimental designs for biological soft tissues and its application in real-world scenarios is essential to understand their mechanical behavior and make advance in medical research.

1.3.2 Material Modeling of Soft Materials

Material models, such as linear elasticity and hyperelasticity play a crucial role for the characterization of material properties, as these describe a relationship that respresents how a material behaves, e.g, the stress response for an applied strain, or the heat transfer for a defined temperature gradient. For the case of soft materials, hyperelastic models are usually useful candidates, as these models can often predict the behaviour of complex materials under certain limitations. Moreover, hyperelastic models can be used as a foundation for more advance models like viscoelastic and viscoplastic models [3].

Hyperelastic models are useful due to their ease of use and calibration, accesibility in major commercial FE softwares, and computational efficiency. However, these models possess some limitations, such as being accurate for monotonic loading, and not capturing rate effects, i.e., viscoelasticity, or hysteresis during cyclic loading [3].

In this subsection linear elasticity and hyperelasticity constitutive models will be presented based on the overview made by Bergström (2015), followed by some examples from the research papers from the Subsection 1.3.1 to confirm the relevance of these models for medical research.

Linear Elasticity

This model is the most basic approach to represent the small strain of the mechanical behavior of solid polymers, with isotropic elasticity being its most elementary form [3]. In isotropic elasticity, stress is proportional to the applied strain and indenpent of the material's orientation. Hooke's law is frequently the constitutive equation for an elastic material, and one form

$$\epsilon_{ij} = \frac{1+\nu}{E}\sigma_{ij} - \frac{\nu}{E}\sigma_{kk}\delta_{ij}\,, \tag{1.1}$$

was presented by Bergström to define a strain-stress relationship, where the indices i and j take the values of 1, 2, and 3, ϵ_{ij} and σ_{ij} are the strain and stress tensors, and

$$\delta_{ij} = \begin{cases} 1, & \text{if } i = j, \\ 0, & \text{otherwise,} \end{cases} \tag{1.2}$$

is the Kronecker delta function. Similarly, the stress

$$\sigma_{ij} = 2\mu\epsilon_{ij} + \lambda\epsilon_{kk}\delta_{ij}\,, \tag{1.3}$$

can be determined in terms of the strain using Hooke's Law. Key parameters in Equations 1.1 and 1.3 include the Young's Modulus E, Poisson's ratio ν, the shear modulus μ, and the Lame's constant λ. The linear elastic constitutive theory can be formulated with the identification of two material parameters, which can be determined through experimental data. After identifying these two parameters it is possible to calculate any other constants. A typical experimental method to identify and calibrate a pair of parameters is the uniaxial tension test, where the stress-strain response identifies E and ν. A significant drawback of using a linear elastic model to predict the mechanical behavior of soft polymers is that these materials exhibit linear behavior only within small strains and limited range of strain-rates and temperatures [3].

Anisotropic Elasticity

Anisotropic elasticity is an extension of linear elasticity theory that considers the anisotropic behavior of the material, as is usually the case for biopolymers. The strain and stress

$$\epsilon_{ij} = S_{ijkl}\sigma_{kl}, \tag{1.4}$$

$$\sigma_{ij} = C_{ijkl}\epsilon_{kl}, \tag{1.5}$$

can be written using Hooke's Law for an anisotropic material. These equations shows that the stress and strain tensor are linearly dependant on each other by a linear stiffness C_{ijkl} or compliance tensor S_{ijkl}. The stiffness and compliance tensors possess 81 components and since the stress and strain tensors are symmetrical the independant components of S and C can be then reduced to 36. Depending on the degree of anisotropy, these matrices can be further simplified.

Hyperelasticity

Hyperelastic models are an extension of linear elasticity that accounts for nonlinearity and large strain predictions. These models have been widely develop over the years and are available in various FE softwares. Hyperelastic models are very important in modeling soft tissues as they can be sometimes connected to the micromechanisms driving the deformation behavior of the material [3]. Some common hyperelastic models include the Neo-Hookean, Mooney-Rivlin and Ogden models.

Neo-Hookean Model

The Neo-Hookean (NH) model is a simple hyperelastic model based on the shear modulus μ and the bulk modulus κ. This model can be used for compressible and incompresible deformations, with the compressible version often being more practical for finite element simulations. The NH model is primarily used for solid, rubber-like materualas characterized by an almost incompressible behavior. Because of this characteristic, the actual value has very small effect on the response of the observed material [3].

The NH model is like other hyperelastic models specified by its Helmholtz free energy per unit reference volume

$$\psi(I_1^*, J) = \frac{\mu}{2}(I_1^* - 3) + \frac{\kappa}{2}(J-1)^2, \tag{1.6}$$

where I_1^* is the distortional first invariant, and J the Jacobian of the deformation gradient [25]. This equation is not adequate for the accurate description of large-strain nonlinear responses. In addition, this equation is not dependant from the second invariant I_2^*, which limits the stress prediction for biaxial loading.

The Cauchy stress for compressible NH model can be expressed as [25]

$$\sigma = \frac{\mu}{J}\mathrm{dev}[\boldsymbol{b}^*] + \kappa(J-1)\boldsymbol{I}\,, \tag{1.7}$$

where $\boldsymbol{b}^*$ left Cauchy-Green strain tensor and $\boldsymbol{I}$ is the identity matrix. The Cauchy stress expressions for uniaxial, planar and biaxial deformations for incompressible NH models are

$$\sigma_{\text{uniax}} = \mu(\lambda^2 - 1/\lambda), \tag{1.8}$$

$$\sigma_{\text{planar}} = \mu(\lambda^2 - 1/\lambda^2), \tag{1.9}$$

$$\sigma_{\text{biaxial}} = \mu(\lambda^2 - 1/\lambda^4), \tag{1.10}$$

respectively. In these equations λ represents the stretches of the deformation [25]. An alternative formulation of the NH model, where the stress is not divided into deviatoric and volumetric parts, is given by

$$\sigma = \frac{\mu}{J}(\boldsymbol{b} - \boldsymbol{I}) + \kappa(J-1)\boldsymbol{I}. \tag{1.11}$$

The predictions from the standard NH model (Eq. 1.7) and this alternative formulation (Eq. 1.11) becomes different with the decrease of the bulk modulus. The main advantage NH model lies in its simplicity; with shear modulus known, the response of most any loading mode can be determined in a robust, and computationally efficient way. However, the limitations of the model lies in capturing large-strains or when the loading is primarily biaxial [3].

The Neo-Hookean model have been employed in various research papers to characterize soft tissue behavior. For instance, in a study from Kanyanta and Ivankovic (2010) used and compare different hyperelastic models to characterize different loadings of an ether-based polyurethane (see Subsection 1.3.1). Here the elastomer was assumed to be an isotropic, incompressible material for the description of the behavior of polyurethane [13].

Furthermore, Chai et al. (2013) utilized the Neo-Hookean model to calculate the Young's modulus of human carotid plaques assumin an isotropic, incompressible model. This knowledge contributes to the identification of local biomechanical properties of atherosclerotic plaque tissue for more reliable rupture risk prediction [5].

In another study made by Shi et al. (2019) a compressible NH model was used to describe the ground substance of the fiber network of the cervical stroma, to identify the μ and λ and then calculate the Young's modulus and Poisson's ratio [21].

Mooney-Rivlin

The Mooney-Rivlin (MR) mode is a model that builds upon the NH model by incorporating a linear dependence on the second invariant I_2^* in the Helmholtz free energy per unit reference volume equation

$$\psi(C_{10}, C_{01}, \kappa) = C_{10}(I_1^* - 3) + C_{01}(I_2^* - 3) + \frac{\kappa}{2}(J-1)^2 \,, \tag{1.12}$$

where C_{10}, C_{01}, κ are the necessary material parameters for the compressible MR model [3]. These parameters are defined based on the experimental data and in case of small strain the shear modulus can be represented as [25]

$$\mu = C_{10} + C_{01} \,. \tag{1.13}$$

The Cauchy stress for the MR model can be expressed as

$$\sigma = \frac{2}{J}(C_{10} + C_{01} I_1^*)\boldsymbol{b}^* - \frac{2C_{01}}{J}(\boldsymbol{b}^*)^2 + [\kappa(J-1) - \frac{2I_1^* C_{10}}{3J} - \frac{4I_2^* C_{01}}{3J}]\boldsymbol{I} \,. \tag{1.14}$$

For the incompressible version of the MR model, the Cauchy stresses in uniaxial, planar and equibiaxial deformations are

$$\sigma_{\text{uniax}} = 2(\lambda^2 - 1/\lambda)[C_{10} + C_{01}/\lambda] \,, \tag{1.15}$$

$$\sigma_{\text{planar}} = 2(\lambda^2 - 1/\lambda^2)[C_{10} + C_{01}] \,, \tag{1.16}$$

$$\sigma_{\text{biaxial}} = 2C_{10}(\lambda^2 - 1/\lambda^4) + 2C_{01}(\lambda^4 - 1/\lambda^2) \,. \tag{1.17}$$

The Mooney-Rivlin model often enhances the accuracy of the predictions of the Neo-Hookean model. However, certain loading modes can cause instability in the case of a negative C_{01} term [3].

Some of the research papers, which used the Mooney-Rivlin model are, e.g., Drass et al. (2018) utilized the MR model to describe the behavior of silicone and identify the hyperelastic parameters through inverse methods. This model showed adequate results for the fitting of four different experimental methods; uniaxial tension and compression test, biaxial tension, and shear pancake test [7].

Likewise, this model proved to be appropiate to simulate the nonlinear properties of breast soft tissues deformation during a leaning forward position and running movement. By identifying the breast properties the bra-breast contact mechanism could be analyzed [22].

Yeoh Model

The Yeoh model (YM) is another hyperelastic model that utilizes a Helmholtz free energy in a third-order polynomial in I_1^* and independent of I_2^*. This allows the the model to provide more accurate predictions than the NH model while potentially avoiding the stability issues of the MR model [3]. The Helmholtz free energy per unit reference volume for a compressible YM can be written as

$$\psi(C_{10}, C_{20}, C_{30}, \kappa) = C_{10}(I_1^* - 3) + C_{20}(I_1^* - 3)^2 + C_{30}(I_1^* - 3)^3 + \frac{\kappa}{2}(J-1)^2 \,, \tag{1.18}$$

where C_{10}, C_{20}, C_{30}, and κ are the material parameters to describe this model. The Cauchy stress for the YM can be derived as

$$\sigma = \frac{2}{J}(C_{10} + 2C_{20}(I_1^* - 3) + 3C_{30}(I_1^* - 3)^2)\text{dev}[\boldsymbol{b}^*] + \kappa(J-1)\boldsymbol{I} \,. \tag{1.19}$$

The indenpendence from the I_2^* term is the main motivation for the Yeoh model. Due to the difficulty of experimentally determining the dependence of this term with the Helmholtz free energy, the neglection of this term in the YM makes is easier that that the hyperelastic model is Drucker stable and therefore, facilitates its use [3]. For the incompressible version of the Yeoh model, the Cauchy stresses in uniaxial, planar, and equibiaxial deformations can be written as

$$\sigma_{\text{uniax}} = 2[C_{10} + 2C_{20}(I_1 - 3) + 3C_{30}(I_1 - 3)^2](\lambda^2 - 1/\lambda)\,, \tag{1.20}$$
$$\sigma_{\text{planar}} = 2[C_{10} + 2C_{20}(I_1 - 3) + 3C_{30}(I_1 - 3)^2](\lambda^2 - 1/\lambda^2)\,, \tag{1.21}$$
$$\sigma_{\text{biax}} = 2[C_{10} + 2C_{20}(I_1 - 3) + 3C_{30}(I_1 - 3)^2](\lambda^2 - 1/\lambda^4)\,. \tag{1.22}$$

The Yeoh model has been proven to improve the prediction of the Neo-Hookean model in various loading modes, specially in large strain scenarios. Bergström also mentions, that for the identification of the material parameters C_{10} should be positive and C_{20}, and C_{30} can be calculated as

$$C_{20} \approx -0.01C_{10}\,, \tag{1.23}$$
$$C_{30} \approx -0.01C_{20}\,. \tag{1.24}$$

In the research of Kayanta and Ivankovic (2010), several constitutive models were compared for the description of polyurethane under different loadings. The results the Yeoh model showed the best fit to the variety of experimental data, however, the Neo-Hookean model showed to be adequate with small strain deformations [13]. Additionally, Łagan et al. (2017) used the Yeoh model to analyze the accuracy of model fitting to the experimental data and estimate the mechanical properties of swine skin tissue in the abdominal region under uniaxial testing [27].

Ogden Model

The Ogden model (OM) is a highly general hyperelastic model that is determined in term of the applied principal stretches [3]. Similar to the previous models, the Helmholtz free energy per volume can written in various ways,

$$\begin{aligned}\psi(\lambda_1^*, \lambda_2^*, \lambda_3^*) = &\sum_{k=1}^{N} \frac{2\mu_k}{\alpha_k^2}((\lambda_1^*)^{\alpha_k} + (\lambda_2^*)^{\alpha_k} + (\lambda_3^*)^{\alpha_k} - 3) \\ &+ \sum_{k=1}^{N} \frac{1}{D_k}(J-1)^{2k}\,,\end{aligned} \tag{1.25}$$

being this equation, one of the most common for a compressible Ogden Model. Different from the previous presented models, is that the volumentric response is not defined by the bulk modulus, but instead D_k parameters. In this equation μ_k, α_k, λ_i^* are material parameters [25]. λ_i^* are the deviatoric principal stretches defined as

$$\lambda_i^* = \frac{\lambda_i}{J^{1/3}}\,, \tag{1.26}$$

where, λ_i are the principal stretches of the left Cauchy-Green tensor [2]. In addition, the initial bulk modulus can be defined from the incompressibility parameter D_1 as

$$\kappa = \frac{2}{D_1}\,. \tag{1.27}$$

Equation 1.25 make the Ogden model versatile but can be complicated when selecting an appropiate set of material parameters that give stable predictions for the deformation states [3]. The principal σ_i stresses can be expressed as

$$\sigma_i = \frac{2}{J}\sum_{k=1}^{N}\frac{\mu_k}{\alpha_k}((\lambda_i^*)^{\alpha_k} - \frac{1}{3}[(\lambda_1^*)^{\alpha_k} + (\lambda_2^*)^{\alpha_k} + (\lambda_3^*)^{\alpha_k}]) + \sum_{k=1}^{N}\frac{2k}{D_k}(J-1)^{2k-1}, \tag{1.28}$$

and the stresses for incompressible OM in unixial, planar and biaxial loading are given by

$$\sigma_{\text{uniax}} = \sum_{k=1}^{N}\frac{2\mu_k}{\alpha_k}[\lambda^{\alpha_k} - (1/\sqrt{\lambda})^{\alpha_k}], \tag{1.29}$$

$$\sigma_{\text{planar}} = \sum_{k=1}^{N}\frac{2\mu_k}{\alpha_k}[\lambda^{\alpha_k} - (1/\lambda)^{\alpha_k}], \tag{1.30}$$

$$\sigma_{\text{biax}} = \sum_{k=1}^{N}\frac{2\mu_k}{\alpha_k}[\lambda^{\alpha_k} - (1/\lambda^2)^{\alpha_k}]. \tag{1.31}$$

The Ogden model turns equal to the Neo-Hookean model when $N = 1$ and $\alpha_2 = 1$. Moreover, the OM shows often a better prediction than the Neo-Hookean and Mooney Rivlin models but is not accurate as the Yeoh model [3].

Ahanchian et al. (2017) applied the first-order Ogden model to investigate the biomechanical behavior of human skin, particularly for the plantar heel pad tissue. This reasearch led to a better understanding the transfer of the load during walking when the foot impacts the floor, and it implication in the design of shoe soles [1].

1.3.3 Inverse Finite Element Method for Parameter Identification

An inverse finite element (FE) approach requires usually a certain experimental model, which generates certain information e. g. load-displacement curve, and through a verified computational model match the given data curve to obtain further information of the material's behavior e. g., stress-strain curve.

Specially for nonlinear cases [11], where the complexity of the problems increases, and the interest is focused to generate an action which results in a certain output response, is where an inverse finite element approach can be helpful to discover a certain variable going from an ouput data. Through an iterative process it is possible to describe the material's behavior and validate the output data it through other established testing e. g., uniaxial testing.

Though this approach does not always give a hundred percent match in all obtain points or zones, it allows the researcher to understand the influences of certain parameters for the materials. This is specially useful for complex materials as biomaterials.

Biomaterials, as mentioned previously, depends on multiple external factors, e.g., blood pressure, affected diseases and the their material properties is constantly changing. This issue does not allow the researcher to develop a proper material model which is usable for multiple use-cases.

Therefore, the importance of the inverse element method as relevant key for estimating constantly changing parameters in soft materials.

For biomechanical models, where the models require knowledge from local properties [5], as the biomaterial is not isotropic; it is possible to identify a parameter e.g.

Young's Modulus from a 3D model. The model can be matched to multiple experiments and multiple samples in different areas, which allows a better representation of the material for further analysis.

The inverse FE approach can used by optimizing the searched parameter by matching the simulated data to a section of a experimental curve and extending this process through some iterations. Nevertheless, it is important to clarify that this method also requires making assumptions to some values. Furthermore, it is relevant to document these assumptions for the further analysis. With the combination of assumptions, experimental data, and a optimized and matched simulation curve, it is possible to solve the complexity of biomechanical models.

In next sections some of the experimental models and the material models for bio and soft materials are going to be explained to get a further understanding in how is possible to get a realiable computational model for further reasearch

Synthetic Soft Materials

Synthetics materials are commonly used to validate an inverse parameter identification process. Usually these synthetic, soft materials provide similar mechanical behavior to it's biomaterials counterparts. This characterization allows to validate a proposed inverse finite element approach process before its applicatoin with a biomaterial, where the measurements to gather the experimental data are some in vivo, and more challenging to recreate.

For example, Silgel, a very soft gel-like material [14] was used for the experimental validation of the inverse finite element method proposed, to characterized the tissue of a human uteri. In this work, the tensile behavior of the material was predicted through the parameters obtained in the aspiration method. The matching procedure is optimize through an objective function, which consists of the squared differences between the simulation and exprimental data. With an optimization algorithm an optimal set of the following parameters was found: the material parameters μ_i [N/m^2] and the bulk Modulus κ [N/m^2]. This method showed good prediction quality of the mentioned material parameters.

Biomaterials

Biomaterials as mentioned before, represent a challenge due its difficult access and lesser replicability. Therefore these materials are usually used for the experimetnal validation of a methd applied previously in synthetic materials. Following the first example of the Silgel in the previous section, the inverse finite element parameter estimation is applied now on human uteri [14] through in vivo and ex vivo measurements of the human tissue of different patients. It was mentioned, that in comparison from the silgel the uterus possesses a complex multi layered structure with strongly anistropic and viscoelastic properties. Nevertheless, five material parameters were determined, based on the strain energy function to model a human uterus (Yamada 1970). Through the same inverse method applied with the synthetic material, the obtained parameters facilitated the prediction of stress-elongation curves for tensile experiments. The resulting curves showed the difference of stiffness for in vivo and ex vivo measurements and the material singurality for each uterus.

1.4 Overview

2 Experimental Model

The first phase of this project was to design and select an appropriate experimental model. This was essential to gather the necessary data from the tested material. This data will be used to determine the design parameters that can help to characterize the material's mechanical behavior.

The experimental model I had the purpose of serving as a comparator for the experimental model II (see Section 2.2). At the beginning of the project, the desired experimental model to be analyzed was the second experimental model, which was developed and designed by Yokohama National University (YNU). As this second experimental model was still undergoing some improvements and corrections, a similar experiment was designed which could fulfill the same purpose.

The chosen experimental characterization for the inverse finite element method for the identification of material parameters for this project was indentation. The goal of these experiments was to observe the mechanical behavior of a soft material under compression using a rounded indenter. The aim was to determine the material behavior and observe the response under an indentation larger than the indenter radius. Additionally, by performing the indentation tests, the obtained data helped for a more in-depth understanding of the material's mechanical behavior for the chosen use cases and the determination of the main assumptions for the material modeling. The main advantage of indentation is the noninvasive feature, which will mostly become useful when a test sample should not be modified, e.g., an organ.

For both experimental setups, the specimen, which was tested, was made from a human skin gel. The human skin gel material was a two-component ultra-soft urethane resin. Polyurethane is widely used for biomedical applications, e.g., preparation of implants, wound dressings, artificial organs, and medical supplies.

Polyurethane can also be used for simulating organ tissues, as it can be tailored to mimic and match the mechanical properties of the desired biological tissues [23]. Furthermore, polyurethane can be synthesized to have a wide range of stiffness, elasticity, viscoelasticity, and can also be prepared with complex shapes for medical research purposes [12].

In this chapter, the different experimental models, which were used to evaluate the mechanical behavior of the ultra-soft polyurethane, will be described. In the first two subsections, will focus on the description and procedure of the experimental models, followed by explanation of the indentation test types. Consequently, an evaluation and analysis of the results will be provided and the main assumptions for the design of the material modeling will be defined.

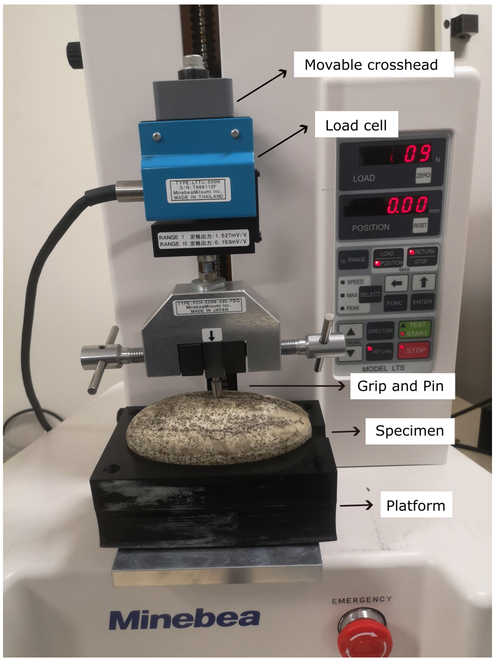

(A) Indentation test configuration with a 500 N load cell

(B) Indentation test configuration with a 10 N load cell

FIGURE 2.1: First experimental model: Tensile and compression machine with an indenter with a rounded head. Test Specimen made from ultra-soft polyurethane resin positioned on a fixed platform with a similar shape for constraint.

2.1 Experimental Model I

Description of the Experimental Setup

The first indentation test configuration was done by adapting a tensile and compression testing machine, model LTS - 500 NB from MinebeaMitsumi.Inc (Fig. 2.1). This machine possess a maximum load capacity of 500 N, and test speeds of 10 mm/min, 20 mm/min, 30 mm/min, 50 mm/min, 75 mm/min and 100 mm/min. To achieve an indentation testing configuration, a pin was attached to the movable crosshead holding grip, as shown in Fig 2.1a. The indenter had a rounded head made of stainless steel with a radius of $r_{i1} = 3$ mm and a length of $l_{i1} = 11$ mm.

The specimen possesses a ellipsoidal form with with a minor radius $r_1 = 35$ mm and a major radius $r_2 = 60$ mm. This specimen geometry is supposed to simulate a kidney with an extracted tumor; therefore, on the lower part of the specimen a half ellipsoid with a minor radius $r_{l1} = 10$ mm and a major radius $r_{l2} = 15$ mm was removed (Fig. 2.2). The specimen was prepared by a YNU laboratory member, by 3D printing a mold with the wanted dimensions and a ellipsoidal shape, and filling it with liquid resin. Additionally, it was left to cure for around 30 hours. It is relevant to clarify, that this sample had been created months before the development of this experimental setup and had been utilized in other projects conducted from the laboratory. This available specimen was positioned on a platform fixed to the base, which suited the ellipsoidal geometry for properly constraint.

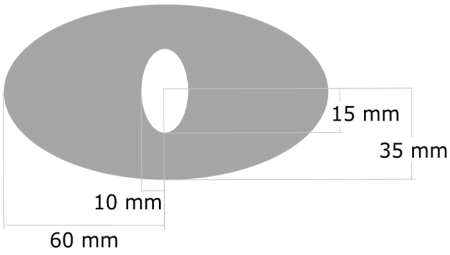

(A) Specimen dimensions bottom view

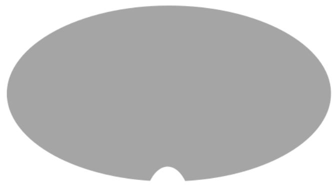

(B) Specimen side view

FIGURE 2.2: First experimental model: Specimen dimensions made from ultra-soft polyurethane resin for indentation test.

Procedure for Conducting the Experiment

For the indentation test after placing the specimen on the platform, the indenter was positioned slightly on the surface of the point of interest. The test was conducted with a room temperature of approximately 22 °C To perform the test the indenter was then lowered onto the surface of the specimen at a velocity of 10 mm/min. The indentation depth was controlled by limiting the maximum depth, and the test stopped once the inserted depth was reached. The indenter returned to its original position after reaching the maximum depth with a rate of 100 mm/min. Due to the material properties, the specimen returned to its original shape. The result of the indentation test was a load-displacement data, which was recorded with a sampling rate of 63 Hz using a load cell of ±500 N and a encoder to measure the displacement.

The measurement accuracy according to the specification of the machine, has a relative reading error of 1.0 %. The indentation test was repeated five times on the same sample to ensure and observe reliability and repeatability. Furthermore, the raw data collected from the test was processed and analyzed using Excel.

During the initial indentation test using the 500 N load cell, the collected experimental data showed noise that could affect the accuracy and reliability of the results. The noise was likely caused by sensitivity of the lead cell. The ultra-soft polyurethane material showed force readings, which were near the lower limit of the load cell's range, which adding any other external factors, results in noisy measurements. To address this issue, a load cell of 10 N was installed (Fig. 2.1b). This change improved the quality of the measurements and reduced the noise in the data. The change to the load cell had some implication to the experimental setup, such as removing the holding grip, and designing a part which could connect the indenter with the new load cell. In addition to changing the load cell, a simple filtering method was used to improve the experimental data. After applying the filter, the noise in the data was reduced, resulting in more smoother force reaction readings.

The applications of the combinations helped to improved the quality and acuracy of the data and gave important information about possible measurement errors to take into consideration for of the experimental model designed by YNU. At last, The filtered data was used for subsequent analysis and interpretation for the inverse finite element method approach for the material parameter identification.

2.2 Experimental Model II

The second experimental model was developed and designed by Yuta Mori, a member of the Yamada Laboratory from the Mechanical Engineering department of Yokohama National University. The main aim for this experimental method was to be able to identify the physical properties of organs in a state that closely resembles the in vivo environment. Additionally, this model seeked two achieve two objectives: firstly, to develop a loading system to acquire the data required for an inverse analysis, and secondly, to establish a measurement process in case of a total nephrectomy [17].

Furthermore, for the present experimental setup a new sample was prepared using the same material as the previous one, i.e., human skin gel made from ultra-soft polyurethane resin, and following the same manufacturing processs as decribe in Section 2.1.

The resulting data from the experimental model served for the basis of the material parameter identification for the inverse finite element method approach. The processed data obtained from this experimental model assisted in the calibration and assessment of the design parameters was employ in the validation for the computational model.

Description and Procedure of the Experimental Setup

In this experimental model the indentation loading system, which gathers data of the indentation depth, reaction force and general deformation. The experimental device consists of an 6-axis force sensor, a laser displacement transducer, and 3D cameras placed in four directions to obtain the point cloud data based on the coordinate system of each camera. Fig.2.3 shows the setup of the experiment. For our project, the 6-axis force sensor and the laser displacement were mainly used. The loading system is operated by specifiying de movement of the loading rod in advance, and the indentation is performed in the direction normal to the contact surface to prevent slippage (Fig. 2.4).

The specimen, same as in the first experimental model (Section 2.1), possessed the same dimensions, a minor radius $r_1 = 35\,\text{mm}$ and a major radius $r_2 = 60\,\text{mm}$, and was made from ultra-soft polyurethane resin. Consequently, the platform is also bowl-shaped. For this experiment, the platform base was made from transparent acrylic resin to record the contact status of the bottom surface [17]. The maximum load capacity of the load cell is 200 N and a theoretical force resolution of 0.001 N. In addition, the resolution of the laser displacement sensor is 0.05 mm. The indenter is sphere-shaped with a radius of $r_{i2} = 3\,\text{mm}$ and was made from ruby with the following specifications; a Young's Modulus of $E_{i2} = 440\,\text{GPa}$ and a Poisson's ratio of $\nu_{i2} = 0.3\,\text{mm}$.

The indentation test was conducted under room temperature conditions. Also, the sample was placed on acrylic platform and the indenter was lowered at constant velocity of 30 mm/min. The experiments were conducted for each loading point five times on the same sample, and the average of the results were calculated.

Furthermore, to minimize the friction during the indentation processs, the indenter and the loading surface on the specimen were covered with a thin layer of lotion. This was done due to inaccuracies and step-like data shown in the measurements. Therefore, to reduce this measurement error, the application of lubricant was

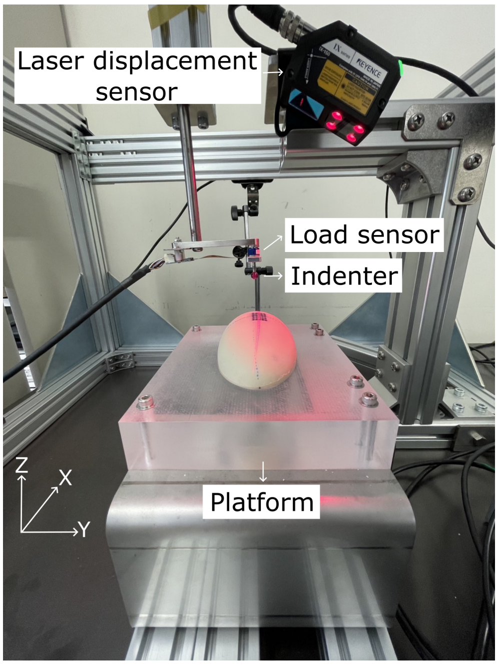

(A) Indentation test configuration front view

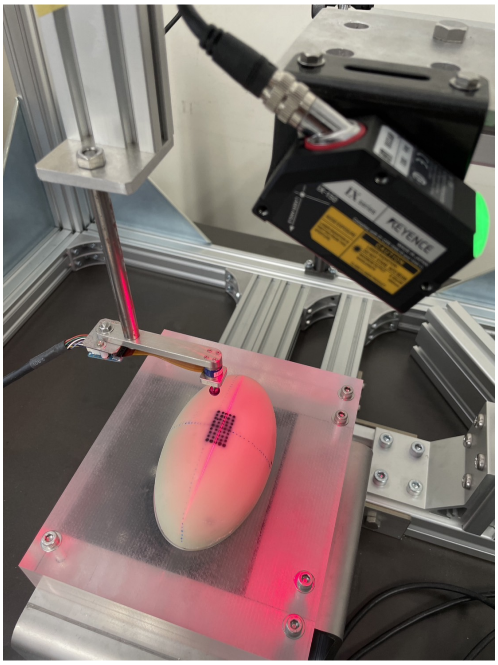

(B) Indentation test configuration top view

FIGURE 2.3: YNU experimental model: 6-axis sensor Test Specimen made from ultra-soft polyurethane resin positioned on a fixed platform with a similar shape for constraint.

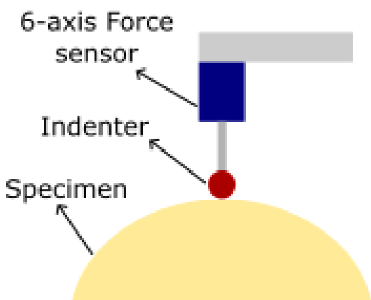

FIGURE 2.4: YNU experimental model: Loading diagram showing initial position of the indenter in normal position [17].

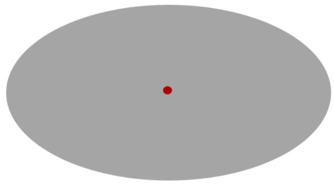

FIGURE 2.5: Middle test point: Loading point (Red point) on the top surface of the specimen.

employed, ensuring a smoother and more controlled indentation process. Finally, the data was also processed and assessed using Excel.

Analysis and Comparison of Experimental Techniques

The second experimental model offers some advantages over the first model. Firstly, it enables not only the measurement of the total force reaction, but also the analysis of the force reaction components F_x, F_y and F_z. This allows for a better understanding of the material's mechanical behavior, as it allows the identification of a specific contribution of the force components and it contributes to identify other mechanisms such as viscoelasticity, plasticity, and creep. In addition, the second model allowed for the measurement of the deformation in other points near the tested loading point. This provides additional information of the material parameters, as it facilitates the characterization of the deformation behavior beyond the direct vicinity of the indentation point. Furthermore, only this test configuration makes use of a lubricant, as this experimental setup could show some inaccuracies in the first data sample.

In contrast, the first experimental model only measures the total force reaction against the indentation depth, without providing any information about the contribution of each component. While the first model allows the data gathering in simpler and more straightforward way, it may not capture the whole complexity of the material.

2.3 Experimental Tests Description

2.3.1 Middle Point

The first use case for the indentation test was performed at the midpoint of the major and minor axis of the ellipsoid (Fig. 2.5). This point was selected to ensure that the indentation was normal to the surface, thereby avoiding the influence of potential shear forces which could influence the measurements.

Additionally, the first indentation depth was chosen arbitriarily, for the first experimental model was $h_I = 3.8\,\text{mm}$, and for the second experimental model was $h_{II} = 4\,\text{mm}$. This depth was considered to be an appropiate compromise that would allow to capture the nonlinear behavior of the material, while also remaining a simple use case to reproduce in a computational model in ANSYS.

As the main objective is to find a path, which lets identify the material parameters, the most basic use case was selected and from this point the complexity was gradually built on. Through this approach, it was possible to establish a solid foundation for the subsequent experiments and data analysis.

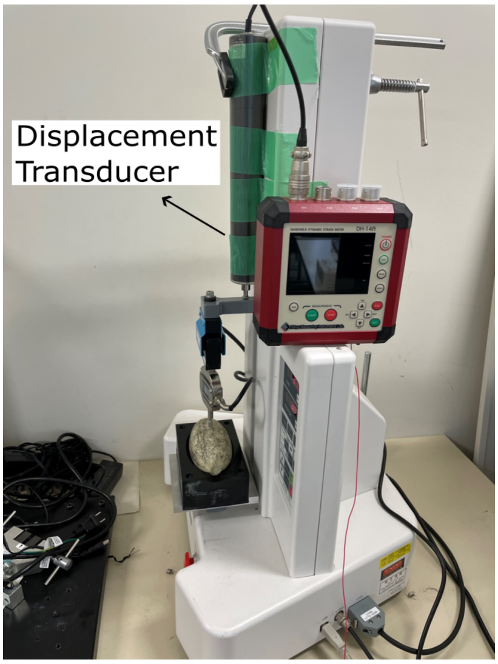

FIGURE 2.6: Load-Unload Case: Experimental model I with modified configuration setup, on top of the movable crosshead a displacement transducer was equipped to capture unloading data.

2.3.2 Load-Unloading

Building on the previous test point (Fig. 2.5), an indentation test was condunted on the same point, with the an indentation depth of 4 mm, but this time in a loading-unloading case.

The first experimental model setup, as describe in Section 2.1, was unable to measure the displacement and force reaction during the unloading of the specimen. As a result, certain modifications were made to the experimental setup. Due to time constraints, the modification of experimental model I was also executed by laboratory members Mori Yuta in YNU. To capture the displacement and force reaction during the unloading, an displacement transducer was equipped to the tensile and compression machine as shown in Figure 2.6.

The aim of this use case, was the observation of a possible hysteresis behavior, as well as to investigate the viscoelastic properties of the material. The load-unload test was performed at six different loading speeds, namely, 10 mm/min, 20 mm/min, 30 mm/min, 50 mm/min, 75 mm/min and 100 mm/min on the same specimen. Each speed configuration was reapeated five times, and te results were average to reduce the effects of experimental variability.

The load-unload case helped to determine whether complex material behavior such as viscoelasticity, could be neglected for the computational model of the middle point test. The result of this experiment were used to make this decision, which has important implications for the simplification of the computational model and its accuracy and reliability.

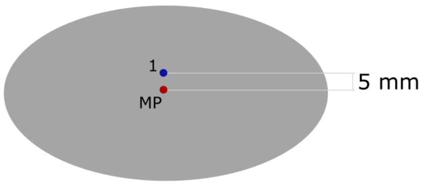

(A) Nearby point location for Experimental model I

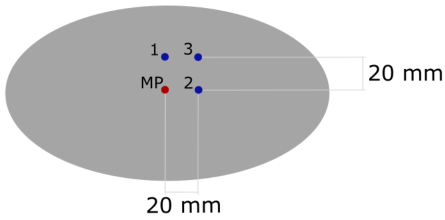

(B) Nearby points location for Experimental model II

FIGURE 2.7: Nearby test point: Loading points for each experimental model to analyze shear stresses and to vbe employed for the validation of the computation models.

2.3.3 Nearby Point

In addition to the indentation performed on the middle point of the surface, further indentations were conducted on nearby points. From these indentation tests, force-displacement curves were recorded. For each indentation the same experiment configuration, e.g., indentation depth and indentation speed, was employed as described in Sections 2.1 and 2.2.

For the first experimental model, only one nearby point located $p_{I1} = 5\,\mathrm{mm}$ to the right of the middle point was selected as shown in Figure 2.7a.

For the second experimental model, three additional nearby points were tested. These points were located at distance of $p_{II1} = 20\,\mathrm{mm}$ to the right, $p_{II2} = 20\,\mathrm{mm}$ downwards, and a third point $p_{II3} = 28.3\,\mathrm{mm}$ diagonally from the middle point forming a square (Fig. 2.7b).

The objective of these testing points was to gain a deeper understanding of the effect of the shear stresses on the indentation response. Furthermore, the results of these points allowed for the validation of the computational model and the selected material model.

2.4 Analysis and Overview of the Data and Results

In this section, the results of the experimental models described in the previous sections will be presented and analyzed. The objective is to understand the behavior of this ultra-soft polyurethane material under indentation and establish the first assumptions for the development of the computational model, as well as the material model. The section will start with a brief summary of the tests, followed by the analysis of the force-stroke curves gathered throughout the experiments.

The experimental model I served mainly as a comparator and a quick way to gain an idea of the mechanical behavior under indentation, for this model three differents use cases were measured. An indentation in the middle point of the surface with and indentation depth of $h_I = 3.8\,\mathrm{mm}$. Subsequently, the load-unload case was observed under an indentation depth of $h_{I2} = 4\,\mathrm{mm}$, and with six different speeds ranging from $10\,\mathrm{mm/min}$ to $100\,\mathrm{mm/min}$. Finally, a nearby point was selected near the middle point, $p_{I1} = 5\,\mathrm{mm}$ to the right, to use it as a validation point for the selected material model.

A similar process was followed for the experimental model II, the middle point indentation was performed with an indentation depth of $h_{II} = 4$ mm and a indentation speed of 30 mm/min, where the force components could be observed. Similarly, the load-unload scenario was tested under the same conditions, and three nearby points were measured.

2.4.1 Middle Point

The results of the indentation test at the middle point for both experimental showed a clear nonlinear behavior. It is assumed that this material possess a elastic-plastic behavior, which in a typical load-displacement curves has four known stages [9]:

1. Nonlinear elastic (self-adjusting): In this stage, the material adjusts itself to the loading conditions, and the deformation is elastic and reversible.
2. Linear elastic: The material is bearing the external load in this stage, the deformation is still elastic and reversible
3. Nonlinear plastic (failing): With the increase of the external load, the material reaches its yield point and undergoes permament deformation
4. Failure: The material fails leading to permanent damage.

Figure 2.8 shows the results of the two indentations at the middle point of the specimen surface. The load-displacement curves showed nearly identical material behavior for both experimental configurations. This use case demonstrate the nonlinear-elastic behavior of the material, as there was no evidence of a yield point or plastic behavior. Both curves began at zero, and the force increased gradually with increasing, resulting in a slightly concave shape.

Figure 2.8a displays all the measurements points obtained from experimental model I and its polynomial approximation. This approximation was used for the subsequent steps of the iFEM approach. The maximum total force for experimental model I at a maximun indentation depth of $u_{I_{MP}} = 3.8$ mm was $F_{I_{MP}} = 0.4218$ N. For experimental model II, at an indentation depth of $u_{II_{MP}} = 4$ mm, the maximum forces for each component were $F_{Z_{II,MP}} = 0.546$ N, $F_{Y_{II,MP}} = 0.0124$ N, and $F_{X_{II,MP}} = 0.0093$ N.

From load-displacement curve of experimental model II (Fig. 2.8b) it was evident that the force reactions in the X and Y directions could be disregard, as these were considerably lower than the force reaction in Z direction. Therefore, the focus in further analysis was mainly on the force reaction in Z direction. Additionally, this case revealed that shear stresses were minimal, which is consistent with the purpose on performing the indentation with the least influence of external factors.

Figure 2.9, shows that the load-displacement curve of experimental model I has a similar initial behavior to that of experimental model II. However, as the indentation depth increases, the curve of experimental model I is positioned lower than that of the second model. One possible explanation for this difference could be the effect of aging on the material properties of the specimen used in the first model. Since the specimen used in this configuration was manufactured months before (Section 2.1), it is possible that the aging had led to a decrease in its mechanical properties, resulting in a lower resistance to deformation and therefore, lower stiffness than the newly manufactured sample. Another possible explanation could be the presence

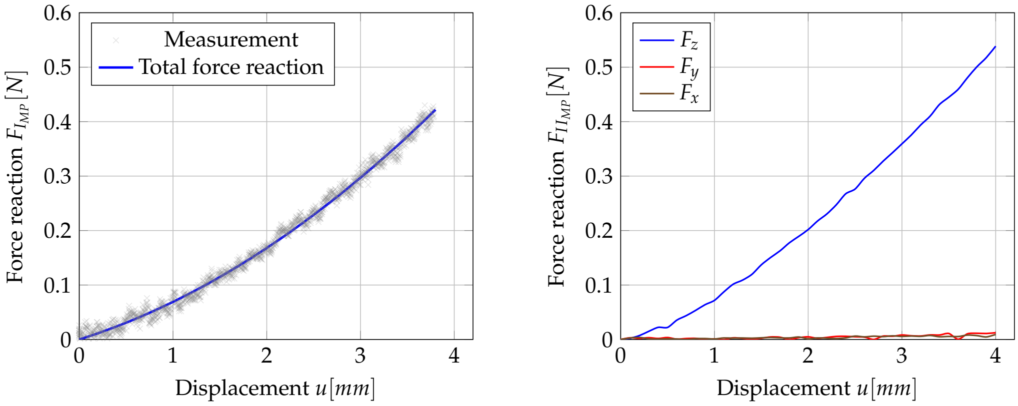

(A) Experimental model I: Total force reaction - indentation depth graph

(B) Experimental model II: Force reaction components - indentation depth graph

FIGURE 2.8: Load-displacement curve experimental data for Middle Point use case for both experimental models.

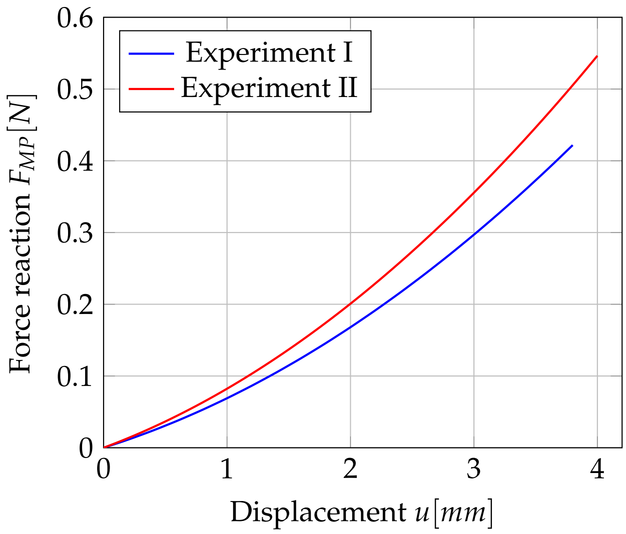

FIGURE 2.9: Total Force Reaction-Displacement curve: Comparison between experimental data for Middle Point use case from both models.

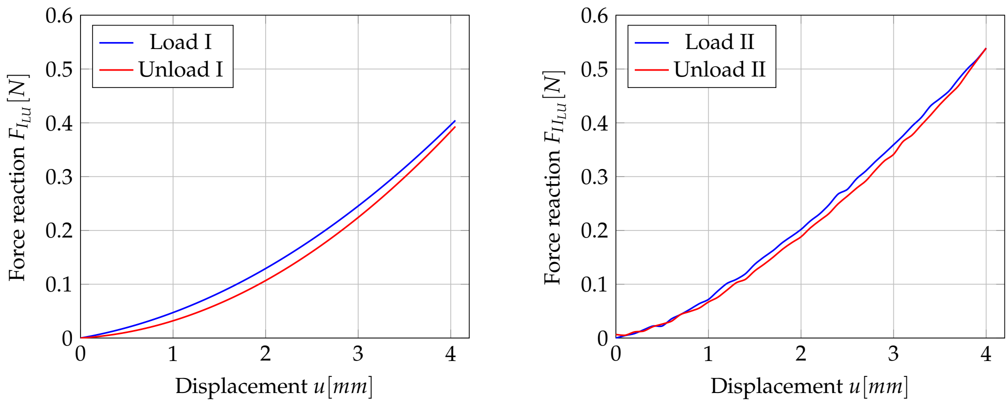

(A) Experimental model I: Total force reaction - indentation depth graph

(B) Experimental model II: Force reaction components - indentation depth graph

FIGURE 2.10: Load-displacement curve experimental data for Load-Unload use case for both experimental models.

of external factors during the conduction of the experiments or the configuration of these. Nevertheless, as the main purpose of this Middle Point use case was to minimize the influence of these factors, this explanation seems less probable.

2.4.2 Load-Unloading

Following the Middle Point use case, in addition to the loading data, the unloading was also captured for both experiments as explained in Section 2.3.2. Figure 2.10 shows the load-displacement curve for experimental model I and next to it experimental model II. Both results exhibited during the unloading some degree of hysteresis, as there was a sligth difference in the force reaction measured. However, the material displayed good elastic behavior, as it returned to its original shape once the indenter was removed.

The hysteresis displayed for both configurations could have occured due to several reasons, such as viscoelastic behavior of the material, or external factors, like friction between the indenter and the specimen, surface roughness of the indenter, test configuration, and so on. To examine closer the main reason for the hysteresis, only with first experimental setup, a series of indentations tests were performed with different speeds.

Figure 2.11 shows the result of the load-unload indentation tests from the lowest to highest value for the indentation speed. It could be observed, that the curves exhibit a similar material behavior. A slight increase in the hysteresis was observed when the indentation speed was increased. Specifically, during the loading, the force reaction were slightly higher as the speed and indentation depth increased. During the unloading, the only notable difference was observed with 100 mm/min, where the unloading curve had the lowest values.

From the results and in the case of ultra-soft polyurethane, it is likely that the hysteresis is primarily due to the viscoelastic behavior of the material. Nevertheless, for the tests done in the middle of the surface, it was decided that the viscoelastic properties could be neglected for the material modeling seeing that the difference between the curves is not impactful for the first stage of the identification of the material parameters.

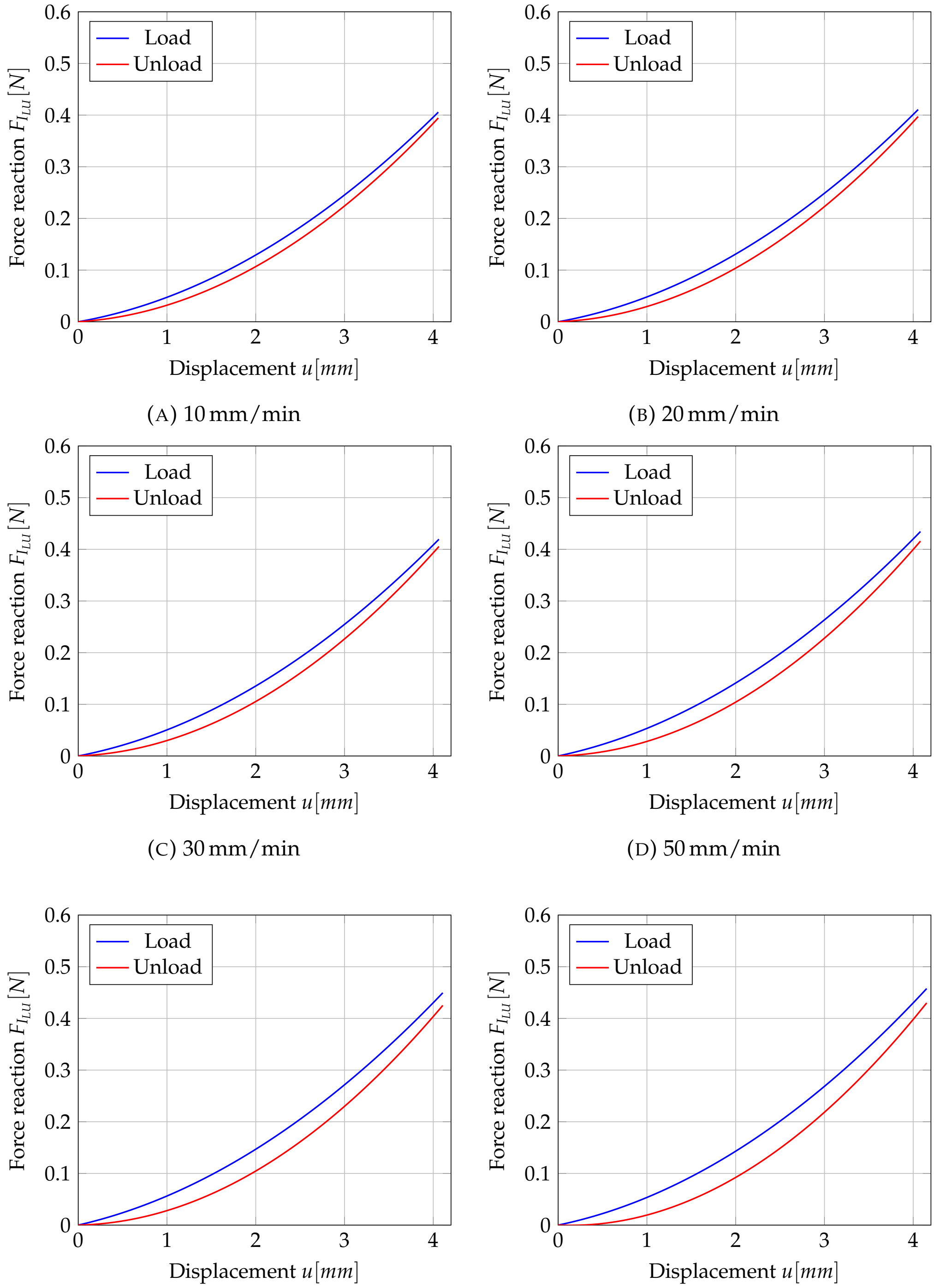

(A) 10 mm/min

(B) 20 mm/min

(C) 30 mm/min

(D) 50 mm/min

(E) 75 mm/min

(F) 100 mm/min

FIGURE 2.11: Load-Unload Use Case: Analysis of Viscoelastic material properties by using six different indentation speeds. Load-Displacement curves were obtained from the first experimental test configuration.

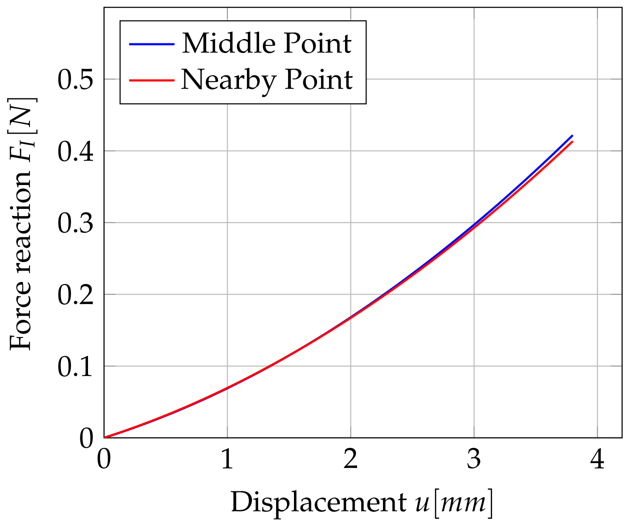

FIGURE 2.12: Total Force Reaction-Displacement curve: Comparison between experimental data for Middle Point and Nearby Point. This point was located 5 mm right from the midpoint, following the minor axis of the ellipsoid.

2.4.3 Nearby Point

To complement the analysis of the viscoelastic behavior of the material, a nearby point located $p_{I1} = 5\,\text{mm}$ to the side of the midpoint, following the minor axis of the ellipsoid (see Subsection 2.3.3). This location was chosen to investigate if the mechanical response of the material is uniform across the surface and if any variations could be detected within a short distance. Figure 2.12 shows the results of the Middle Point use case vs. the selected Nearby Point case for experimental model I.

The new load-displacement shows nearly identical behavior to that of the first case, except for the last part of the curve, where the Nearby Point curve goes slightly lower. The maximum force obtained for the Nearby Point case was $F_{I_{NBP}} = 0.4134\,\text{N}$, which is lower than the one obtained before, which was $F_{I_{MP}} = 0.4218\,\text{N}$.

It can be concluded, that the results from this nearby point support the findings from the Middle point test, indicating that the material behavior was homogeneous in the region of interest. The small difference in the maximum force values could be due to the variations in the experimental conditions, e.g. the increment of the gradient of the contact surface due to the curvature of the specimen. This change could potentially affect the distribution of the stress and strains within the material. Nonetheless, these differences were not significant enough to affect the overall conclusions.

With the measurements taken in the additional nearby points for experimental model II (Subsection 2.3.3), it was possible to investigate whether the small variations in the results obtained with experimental model I could be attributed to the difference in the gradient of the contact surface. Figure 2.13 shows the result for each force reaction component for all four tested points. In X-direction, the maximum force was observe for point 2, which had the smallest gradient contact surface, followed by point 3. These points were 20 mm down along the X-axis, in contrast to the other two points, which were at the origin of the X-axis. For the middle point and point 1, which had the largest contact surface gradient, the X-component force reaction was almost 0 N.

Similarly, in Y-direction, the maximum force was observed for point 3, followed closely by point 1. For the middle point and point 2 the Y-component force reaction was almost 0 N. Point 3 and point 1 were 20 mm right along the Y-axis, and the middle point and point 2 were at the origin of the Y-axis. As for the Z-direction, the maximum force was observed at the middle point, followed by point 2, and consequently with similar results point 1 and point 3. For all the points the results in Z-direction are more significant than in the other directions.

These results suggested that variation in the gradient of the contact surface may have contributed to the small differences in the results obtained with experimental model I. Specifically, it was observed, that with a smaller contact surface gradient the higher the X-component the same for the Y-component with the larger contact surface gradient. In conclusion it is possible to confirm that the material behavior was homogeneous, and that the larger the contact surface gradient became, the lower the total force reaction.

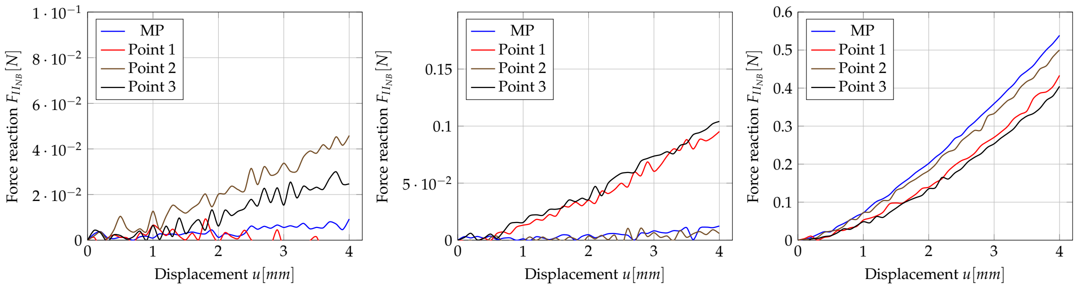

(A) Force in X-direction (B) Force in Y-direction (C) Force in Z-direction

FIGURE 2.13: Nearby Point Use Case: Analysis of shear stresses by observing three different nearby points on the specimens surface. Load-Displacement curves were gathered from Experimental Model II showing each force component.

2.5 Main Assumptions for Material Modeling

In this section, the main assumptions based on the results obtained from the indentation tests will be summarized. These assumptions will be used for the development of the material models. As previously mentioned, one of the goals of this project was to develop the material model from an ideal scenario, while considering the limitations at each level. The complexity of the material model was incrementally increased until a set of material parameters that provided a proper compromise to the experimental results was obtained. Defining these levels allowed the assessment of the impact of each parameter on the development of the material model.

Based on the presented experimental data and previous discussion, the following assumptions could be made:

1. The material can be assumed to be homogeneous in the region of interest for the Middle Point Case, as the results from the nearby points support the findings from midpoint test.

2. Nonlinear elasticity is observed and hysteresis can be neglected, as the changes observed with the different loading speeds were not significant enough to affect the initial results.

3. The viscoelasticity of the material can be ignored for the first design of the material model, as the material returns to its original shape and almost no energy is lost during deformation.

4. Friction and shear stresses will be neglected, as in the Middle Point case the observed force components in x and y directions are non-relevant.

It is important to mention, that it was noted that the main assumptions made may not hold for different experiment settings, such as higher loads, longer loading times, higher temperatures, high shear stresses, and so on. Therefore, it was important to keep these assumptions in mind when using the chosen material model in a validation case.

2.5.1 Level 1: Linear elasticity

The first level a linear elastic model was used. This model assumed that the material behaves linearly, i.e., the deformation is linearly proportional to the applied load and the material returns to its original shape after the load is removed. This model is based on Hooke's law, where the stress-strain relationship is

$$\sigma = E\varepsilon\,,$$

where σ is the stress, E is the elastic modulus, and ε is the strain. For the Middle Point Case, the material is assumed homogeneous and isotropic, thus the elastic modulus is the same in all directions. For an indenter with a spherical tip, the contact area A between the indenter and the specimen can be approximated as,

$$A = r_i^{\frac{1}{2}} h^{\frac{1}{2}}\,,$$

where r_i is the radius of the indenter, and h is the indentation depth. For a spherical indentation assuming the Hertzian contact theory, the Hertzian relationship between the applied force F and the indentation depth h is [15],

$$F = \frac{4E{r_i}^{\frac{1}{2}} h^{\frac{3}{2}}}{3(1-\nu^2)}\,, \tag{2.1}$$

where E and ν are the Young's modulus and Poisson's ratio of the indented material. This Hertzian relationship is used as the analytical basis on the contact of ellipsoid bodies in indentation experiments [15]. This model provided a simple and straightforwards approach to describe the material behavior under small deformations. The elastic modulus and the Poisson's ratio are the two main parameters that will be used for this model. Additionally it was assumed that the material is near incompressible, therefore, a fixed Poisson's ratio was chosen,

$$\nu = 0.49\,, \tag{2.2}$$

leaving the analysis of one parameter, the elastic modulus. The linear elastic model served as a basis for the more complex material models developed in the subsequent levels, and it provided a reference point for the identification of other material parameters.

2.5.2 Level 2: Hyperelasticity

The second level introduces a higher complexity, as more material parameters are analyzed. For this level a Neo-Hookean model was used to describe the material behavior based in the strain energy potential function. The elastic strain energy potential function for the Neo-Hookean material model is given by

$$W = C_1(I_1 - 3) + \frac{1}{D_1}(J-1)^2\,, \tag{2.3}$$

where C_1 is a material constant, D_1 the material incompressibility parameter, J the determinant of the elastic deformation gradiant, and I_1 is the first invariant of the right Cauchy-Green deformation tensor, i.e.

$$I_1 = {\lambda_1}^2 + {\lambda_3}^2 + {\lambda_3}^2\,,$$

where λ are the principal stretches [18]. To maintain conformity with linear elasticity, the material constant

$$C_1 = \frac{\mu}{2}\,, \tag{2.4}$$

where μ is the shear modulus or the second Lamé parameter. If the material is assumed to be incompressible,

$$J = 1\,,$$

and the second term in the strain energy potential W becomes zero [19].

The Neo-Hookean model requires two main parameters to be identified; the shear modulus μ and the incompressibility parameter D_1. The incompressibility parameter relationship with the initial bulk modulus

$$K = \frac{2}{D_1}\,, \tag{2.5}$$

can be defined [2]. The relationship between the shear modulus, the elastic modulus, and the Poisson's ratio

$$\mu = \frac{E}{2(1+\nu)}\,, \tag{2.6}$$

can be calculated, as well as for the bulk modulus

$$K = \frac{E}{3(1-2\nu)}\,. \tag{2.7}$$

Using the results of the first level with E and ν it is possible to establish a possible range for μ and D_1. This targeted range helped in the reduction of computational time for simulations. The hyperelastic model provides a more accurate description of the material behavior in comparison to linear elastic model, as this model takes into account the nonlinear behavior of the material.

3 Computational model

3.1 Middle point

3.1.1 Description

The quasi static nature of the indentation experiment allows the use of a static structural analysis.

For the creation of the computational model, the SOLID 187 elements were used. The mesh for the whole model is formed from quad tetrahedral elemennts. The platform and the specimen have an global element size of 5 mm. The indenter has an element size of 0.5 mm. In the area of the indentation, there is finer mesh with an element size of 1 mm and a radius of 8 mm.

3.1.2 Analysis and Complications

Their a two main factors which increases the complexity of the validation of the simulation and those are, the contact nonlinearity, and the element distortion due to indentation experiment. These issues make the computational time expensive, as it requires to manual solutions for the meshing in the area of importance, and small time steps. For that, the nonlinear adaptive meshing option in ANSYS Workbench was applied, which does a remeshing process if the a certain parameter is exceeded.Specially, for larger indentation cases, this option shows a more stable model with a good mesh convergence analysis.

A force-displacement curve, shown in Fig... is generated from the first assumption, for this case

For both cases

3.1.3 Verification of the Simulation Model

Mesh Convergence Analysis

Platform vs Fixed Support

3.2 Nearby point

4 Inverse Finite Element Method for Material Parameter Identification

4.1 Procedure of IFEM

4.2 Material Modeling

In an ideal and first scenario, this material can be assumed as linear, isotropic, elastic and nearly imcompressible. For this case, there are two main variables, the Young's Modulus E, and the Poisson's ratio ν.

From the parametric analysis, it is possible to see that the bulk modulus of this material does not possess a big impact in the FE simulation results. This conclusion combined with the results from the Poisson ratio in the first material model coincide with the statements from Bergström, where it is no vital to know these parameters to obtain accurate FE computational models, as these have limited influence on the mechanical response. [3]

4.2.1 Response Surface Optimization

Linear Elastic Model

Hyperelastic Model: Neo-Hookean

4.2.2 Objective Function Optimzation

4.2.3 Analysis and Comparison of Each Approach

5 Results

5.1 Overview and Analysis

5.2 Framework proposal

5.3 Verification and Validation

5.3.1 Deeper indentation

5.3.2 Deformation profile analysis

5.4 Limitations and implications of the results

5.4.1 First Experimental model

The chosen experimental technique for the inverse identification for this project was indentation. The test specimen used for this experiment was a ultra-soft polyurethane resin. As shown in Fig.. the specimen possesses a ellipsoidal form with with a minor radius r_1 = 35 mm and a major radius r_2 = 60 mm. This was positioned on a fixed platform that suited the ellipsoidal geometry of the specimen to constrain its movement. The specimen was tested in a indentation test configuration with a tensile/compression machine. To achieve this congiguration a pin with a rounded head made of structural steel, with a radius of r_3 = 3 mm was attached to the holding grips followed by a force load cell. The result of indentation test was a load-displacement points. The approximated polynomial curve was used as a reference for the material modeling.

The measured force reation F_1 data showed a very small number, so the first 50 N load cell displayed a lot of noise in the measurements. Therefore, the load cell was change to 10N to reduce this interference. The 10 N load cell displayed the force-displacement curve of the indenter and the specimen in a finer way. Furthermore, in order to get the measurement of the load and unloading process of the indentation a displacement sensor was attached to the tensile machine.

The indentation depth h_1 selected for the first model was 3,8 mm on the middle of the top surface of the specimen. This indentation depth surpasses the pin radius r_3 and was chose arbitriarily to analyze the behavior of the material on the defined position. Additionally, it was observed that in soft materials it is easier to capture some parameters with a larger indentation. Some references also observe that with indentation depth lower than indenter radius has a lot of noise and do not describe th results accurately.

From the first experimental model we can observe that the material shows a non-linear behavior and the maximum total force reaction F_1 lies around 0.45 N. Furthermore, when applying different speeds, as show in Fig. it is also possible to observe that the hysteresis increases. This increasement shows that the material possesses a viscoelastic behavior, however as this increasement is not significantly, it is possible to neglect viscoelasticity for the first stages of the project.

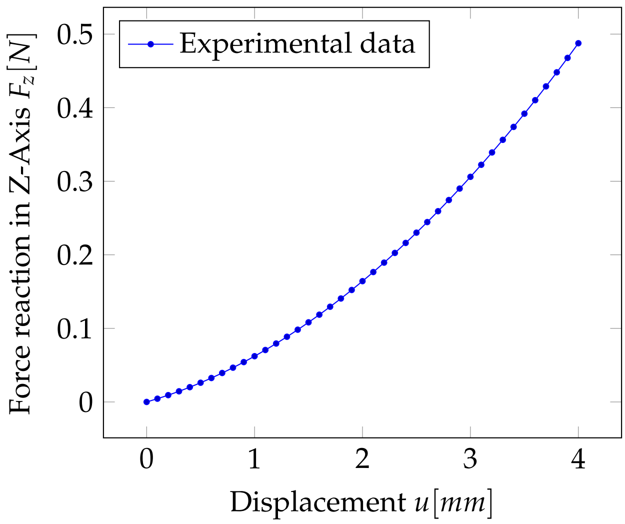

FIGURE 5.1: Experimental Load-displacement curve.

5.4.2 Second Experimental model

The second experimental model was developed by Yokohama National University. Similar to the first experimental model the test specimen and the platform were it lies, has the same dimensions, minor radius $r_1 = 35$ mm and a major radius r_2 of 60 mm. The test specimen is also made from the same material, ultra-soft polyurethane resin.

The indenter on the other hand, is a sphere made of ruby, the sphere radius is also equal to the radius of the pin r_s 3 mm and attached to it, is the force load cell.

A laser is used to measure the displacement which results in a load-displacement curve. With this model it is possible to not only determine the toal force reaction, but also it's components F_x, F_y and F_z. Furthermore, with the laser it is also possible to observe the deformation not only in one point but around the whole area. This allows as to analyze the deformation of the whole structure.

The indentation speed selcted was and with an indentation depth of h_s is 4 mm. With this experiment, 4 key points on the sepcimen's surface were chosen: First, in the middle and three other points, one to right, one down, and one diagonal to middle, forming a square with a distance between points of d_s 20 mm.

Similar to the previous model, Fig. shows a nonlinear behavior with a maximum force reac

5.5 Material model framework assumptions

The first point to be analyzed, which is used to build a material model is point No. 1, in the middle of the surface. The advantages from this case, is the less influence of external factors. For this case it is vaiable to assumed, that shear stresses can be neglected and offers a simple model to focus on the material definition.

For this project, there is a focus on the limitation of each material model, departing from an ideal scenario. From this point on the material will be build accordingly and for each model the influence of the material parameters is going to be assessed.

5.5.1 First Material model

Linear elasticity

Hyperelasticity

The strain energy density function for the Neo-Hookean material model is given with

$$\Psi = C_1(I_1 - 3)\,,$$

where C_1 is a material constant and $I_!$ is the first invariant of the right Cauchy-Green tensor. Neo Hookean and Mooney Rivlin comparison

5.6 Computational model

The quasi static nature of the indentation experiment allows the use of a static structural analysis.

For the creation of the computational model, the SOLID 187 elements were used. The mesh for the whole model is formed from quad tetrahedral elemennts. The platform and the specimen have an global element size of 5 mm. The indenter has an element size of 0.5 mm. In the area of the indentation, there is finer mesh with an element size of 1 mm and a radius of 8 mm.

Their a two main factors which increases the complexity of the validation of the simulation and those are, the contact nonlinearity, and the element distortion due to indentation experiment. These issues make the computational time expensive, as it requires to manual solutions for the meshing in the area of importance, and small time steps. For that, the nonlinear adaptive meshing option in ANSYS Workbench was applied, which does a remeshing process if the a certain parameter is exceeded.Specially, for larger indentation cases, this option shows a more stable model with a good mesh convergence analysis.

A force-displacement curve, shown in Fig... is generated from the first assumption, for this case

For both cases

5.7 Material model

In an ideal and first scenario, this material can be assumed as linear, isotropic, elastic and nearly imcompressible. For this case, there are two main variables, the Young's Modulus E, and the Poisson's ratio ν.

From the parametric analysis, it is possible to see that the bulk modulus of this material does not possess a big impact in the FE simulation results. This conclusion combined with the results from the Poisson ratio in the first material model coincide with the statements from Bergström, where it is no vital to know these parameters to obtain accurate FE computational models, as these have limited influence on the mechanical response. [3]

6 Conclusion and Outlook

6.1 Summary and Contributions

6.2 Recommendations for Future Research

6.3 Conclusions and Final Remarks

A Frequently Asked Questions

A.1 How do I change the colors of links?

The color of links can be changed to your liking using:
`\hypersetup{urlcolor=red}`, or
`\hypersetup{citecolor=green}`, or
`\hypersetup{allcolor=blue}`.
If you want to completely hide the links, you can use:
`\hypersetup{allcolors=.}`, or even better:
`\hypersetup{hidelinks}`.
If you want to have obvious links in the PDF but not the printed text, use:
`\hypersetup{colorlinks=false}`.

Bibliography

[1] Nafiseh Ahanchian et al. "Estimating the material properties of heel pad sublayers using inverse Finite Element Analysis". In: *Medical Engineering and Physics* 40 (2017), pp. 11–19. DOI: 10.1016/j.medengphy.2016.11.003.

[2] "Ansys Mechanical APDL Element Reference". In: (Nov. 2010).

[3] Jörgen Bergström. *Mechanics of Solid Polymers: Theory and Computational Modeling*. ISBN: 9780323311502.

[4] F J Carter et al. *Measurements and modelling of the compliance of human and porcine organs*. 2001, pp. 231–236. URL: www.elsevier.com/locate/media.

[5] Chen Ket Chai et al. "Local axial compressive mechanical properties of human carotid atherosclerotic plaques-characterisation by indentation test and inverse finite element analysis". In: *Journal of Biomechanics* 46 (10 June 2013), pp. 1759–1766. DOI: 10.1016/j.jbiomech.2013.03.017.

[6] Martijn A.J. Cox et al. "Mechanical characterization of anisotropic planar biological soft tissues using large indentation: A computational feasibility study". In: *Journal of Biomechanical Engineering* (3 June 2006), pp. 428–436. DOI: 10.1115/1.2187040.

[7] Michael Drass et al. "Adhesive connections in glass structures—part I: experiments and analytics on thin structural silicone". In: *Glass Structures and Engineering* 3 (1 Mar. 2018), pp. 39–54. ISSN: 23635150. DOI: 10.1007/s40940-017-0046-5.

[8] Yuan Feng et al. "Characterizing white matter tissue in large strain via asymmetric indentation and inverse finite element modeling". In: *Journal of the Mechanical Behavior of Biomedical Materials* (2017), pp. 490–501. DOI: 10.1016/j.jmbbm.2016.09.020.

[9] Amirhossein Goharian, Seyed S.R. Koloor, and Mohamed R. Abdullah. *Biomechanical Evaluation Methods*. Elsevier Inc., Mar. 2017, pp. 65–87. DOI: 10.1016/B978-0-12-804634-0.00005-7.

[10] Michelle Griffin et al. "Biomechanical characterization of human soft tissues using indentation and tensile testing". In: *Journal of Visualized Experiments* (118 Dec. 2016). ISSN: 1940087X. DOI: 10.3791/54872.

[11] Asif Husain, D. K. Sehgal, and R. K. Pandey. "An inverse finite element procedure for the determination of constitutive tensile behavior of materials using miniature specimen". In: *Computational Materials Science* 31 (1-2 Sept. 2004), pp. 84–92. DOI: 10.1016/j.commatsci.2004.01.039.

[12] J. Joseph et al. "Biomedical applications of polyurethane materials and coatings". In: *Transactions of the Institute of Metal Finishing* (3 May 2018), pp. 121–129. DOI: 10.1080/00202967.2018.1450209.

[13] Valentine Kanyanta and Alojz Ivankovic. "Mechanical characterisation of polyurethane elastomer for biomedical applications". In: *Journal of the Mechanical Behavior of Biomedical Materials* 3 (Jan. 2010), pp. 51–62. ISSN: 17516161. DOI: 10.1016/j.jmbbm.2009.03.005.

[14] M. Kauer et al. "Inverse finite element characterization of soft tissues". In: *Medical Image Analysis* 6 (2002), pp. 275–287.

[15] David C. Lin et al. "Spherical indentation of soft matter beyond the Hertzian regime: Numerical and experimental validation of hyperelastic models". In: *Biomechanics and Modeling in Mechanobiology* (Oct. 2009), pp. 345–358. DOI: 10.1007/s10237-008-0139-9.

[16] Kaifeng Liu, Mark R. VanLandingham, and Timothy C. Ovaert. "Mechanical characterization of soft viscoelastic gels via indentation and optimization-based inverse finite element analysis". In: *Journal of the Mechanical Behavior of Biomedical Materials* 2 (Aug. 2009), pp. 355–363. DOI: 10.1016/j.jmbbm.2008.12.001.

[17] Yuta Mori. "Development of a method for identifying the physical properties of post-extraction organs". In: (Feb. 2022).

[18] R.W. Ogden. *Non-Linear Elastic Deformations*. Dover Civil and Mechanical Engineering. Dover Publications, 2013. ISBN: 9780486318714.

[19] Thomas J. Pence and Kun Gou. "On compressible versions of the incompressible neo-Hookean material". In: *Mathematics and Mechanics of Solids* 20 (2 Feb. 2015), pp. 157–182. ISSN: 17413028. DOI: 10.1177/1081286514544258.

[20] Padmanabhan Seshaiyer and Jay D. Humphrey. "A sub-domain inverse finite element characterization of hyperelastic membranes including soft tissues". In: *Journal of Biomechanical Engineering* 125 (3 June 2003), pp. 363–371. ISSN: 01480731. DOI: 10.1115/1.1574333.

[21] Lei Shi et al. "Anisotropic Material Characterization of Human Cervix Tissue Based on Indentation and Inverse Finite Element Analysis". In: *Journal of Biomechanical Engineering* (Sept. 2019). DOI: 10.1115/1.4043977.

[22] Yue Sun et al. "Optimization method for the determination of Mooney-Rivlin material coefficients of the human breasts in-vivo using static and dynamic finite element models". In: *Journal of the Mechanical Behavior of Biomedical Materials* 90 (2019), pp. 615–625. DOI: 10.1016/j.jmbbm.2018.11.016.

[23] Wenshou Wang and Chun Wang. *Polyurethane for biomedical applications: A review of recent developments*. Elsevier, 2012, pp. 115–151. DOI: 10.1533/9781908818188.115.

[24] Chen En Wu, Keng Hui Lin, and Jia Yang Juang. "Hertzian load-displacement relation holds for spherical indentation on soft elastic solids undergoing large deformations". In: *Tribology International* (May 2016), pp. 71–76. DOI: 10.1016/j.triboint.2015.12.034.

[25] George Youssef. *Hyperelastic behavior of polymers*. 2022, pp. 117–144. DOI: 10.1016/b978-0-12-821078-9.00002-8.

[26] Man Gong Zhang et al. "Spherical indentation method for determining the constitutive parameters of hyperelastic soft materials". In: *Biomechanics and Modeling in Mechanobiology* (1 2014), pp. 1–11. ISSN: 16177959. DOI: 10.1007/s10237-013-0481-4.

[27] Sylwia D. Łagan and Aneta Liber-Kneć. "Experimental testing and constitutive modeling of the mechanical properties of the swine skin tissue". In: *Acta of Bioengineering and Biomechanics* 19 (2017). DOI: 10.5277/ABB-00755-2016-02.